PATTERN OF SEISMICITY IN THE LUCANIAN APENNINES AND FOREDEEP (SOUTHERN ITALY) FROM RECORDING BY SAPTEX TEMPORARY ARRAY

Frepoli A., Cinti F.R., Amicucci L., Cimini G.B., De Gori P., Pierdominici S.

Istituto Nazionale di Geofisica e Vulcanologia, Rome, Italy. E-mail: frepoli@ingv.it

in press on Annales of Geophysics (2005)

PATTERN OF SEISMICITY IN THE LUCANIAN APENNINES AND FOREDEEP (SOUTHERN ITALY) FROM RECORDING BY SAPTEX TEMPORARY ARRAY

Frepoli A., Cinti F.R., Amicucci L., Cimini G.B., De Gori P., Pierdominici S.

Istituto Nazionale di Geofisica e Vulcanologia, Rome, Italy. E-mail: frepoli@ingv.it

Abstract

The deployment of a temporary seismic network in southern Italy during 2001-2004 (the SAPTEX array, Southern APennine Tomography EXperiment) allowed us to relocate the hypocenters of southern Apennines earthquakes with low uncertainty among the location parameters. The best array distribution of the SAPTEX network for the analysis of seismicity in the Lucanian Apennines and foredeep was reached in the first two years of recording. The SAPTEX data were merged with those of the Italian National Seismic Network (RSNC) operated by the Istituto Nazionale di Geofisica e Vulcanologia (INGV). For the hypocenters computation of events in the upper Agri Valley, we also included P- and S- waves arrivals from the local ENI-AGIP network. The seismicity for the Lucanian Apennines and foredeep in the analyzed period has magnitudes ranging from 2.0 to 4.1. A major remark is the identification of two different crustal domains: the westernmost characterizing the chain, mostly with shallow earthquakes (within about 20 km of depth), and the easternmost one belonging to the outer margin of the chain and to the foredeep, with deeper seismicity (mostly between 20-40 km of depth). Thirty fault-plane solutions were computed and used for stress inversion; most of them are related to earthquakes within the chain sector and indicate a generalized NE-SW extension. Moreover, the dense network allowed us to improve the location of events relative to two low magnitudes sequences occurred in the study period.

Key words: seismicity, seismic network, seismotectonics, Lucanian Apennines, Lucanian foredeep, southern Italy.

1. Introduction

The SAPTEX passive array was planned by *Cimini et al.* (2005) and represented the longest deployment of portable seismic stations carried out in southern Italy. The main goal of the experiment was to better resolve the crustal and upper mantle structure beneath southern Italy. In fact, the paucity of permanent stations in this region was still remarkable thus preventing high-resolution tomographic studies, detail definition of the lithosphere-astenosphere structure and precise hypocentral determination. The three years long experiment provided the extraction of numerous digital waveforms of local, regional and teleseismic events [for additional details on the network see *Cimini et al*., 2005].

In this work we benefit of using data from SAPTEX temporary stations to analyze the seismicity occurring in the Lucanian area, that is definitively a seismically active area of southern Italy (Figure 1). Based on the instrumental catalogues (1981-2002 from *Castello et al.,* 2005; 2002 to present from *INGV seismic bulletin*), a 30-40 km wide belt of seismicity

characterizes the Lucanian Apennines and its outer margin, where earthquakes reach the highest magnitudes. Conversely, along the external zones of the Bradano foredeep and Apulia foreland, low to moderate-size earthquakes are infrequent and sparse (Figure 1). Most of the earthquakes are limited to the upper crust (hypocentral depths < 20 km), defining the depth extent of the seismogenic layer of this region. A dense cluster of earthquakes surrounds the city of Potenza (referred to as the Potentino area), a second is located in the Irpinia region, and a third cluster is in the northwestern part of the Pollino (referred to as the Castelluccio area). An area of very scarse seismicity extends for about 25 km in the NW-SE direction within the Apenninic chain from the Vallo di Diano and upper Agri Valley. In the last 25 years, the most destructive event is the 1980 Irpinia event (Mw=6.9; see Table 1) with normal mechanism of rupture [*Boschi et al.*, 1990]. A significant earthquake occurred in 1990 (Mw=5.7) in the Potentino area [*Azzara et al.*, 1993; *Ekström*, 1994]; aftershock depths of this sequence range between 15 and 25 km on an E-W oriented strike-slip structure. A similarly located event occurred in 1991 [Mw=5.2; *Ekström*, 1994]. The different focal solutions obtained for the Irpinia inland event and the two external Potentino events, suggest the presence of a transition zone between pure extensional, to the west, and strike-slip regime, to the east. The strike-slip, Mw 5.7, 2002 Molise earthquake located to the east of the chain at 20 km depth [*Di Bucci and Mazzoli*, 2003; *Valensise et al.*, 2004; *Di Luccio et al.*, 2005] would support this setting also northwest of the study area. Finally, the 1998, Mw=5.6 Castelluccio event with pure normal focal mechanism, hit the northwestern side of the Pollino range [*Michetti et al.*, 2000; *Pondrelli et al.*, 2002]. Similarly to the recent seismicity, most of the destructive events reported in the historical catalogue [*CPTI Working group*, 1999] are located within the Apenninic chain (Figure 1); among them, the largest is the 1857 (Ma=7.0) occurring south of Potenza, in the Agri Valley.

The availability of a denser station coverage provided by the SAPTEX array respect to that of the national network RSNC, represented a good opportunity for highlighting details of "earthquake structures" in the Lucanian area and to investigate the region's active tectonics. We could determine high quality hypocentral parameters and fault-plane solution of local earthquakes recorded at the temporary SAPTEX network in the period 2001-2002, merged with the RSNC data and the ENI-AGIP local network (Figure 2). We performed the picking of SAPTEX phases and re-picked those from RSNC seismic network. The ENI-AGIP local network provided us directly the P- and S- time arrivals. The work is developed in the following steps: location of events occurred in the period June 2001 – December 2002, 3D analysis of the seismicity pattern, analysis of sequences, focal mechanisms computation and inversion of fault-plane solutions for stress field determination. In conclusion, we discuss the results integrating the seismic data collected with a seismic profile.

2. Earthquake data

We analyzed the seismicity of the Lucanian region occurred in the time period between June 2001 and December 2002. The earthquakes have been recorded at the SAPTEX temporary array and the RSNC network. For the analysis of the seismicity in the upper Agri Valley and surrounding areas, the P- and S- wave arrival time readings from ENI-AGIP seismic network (Figure 2) were also used. The recording mode of the SAPTEX stations was continuous, while the RSNC and ENI-AGIP networks record as trigger mode. The list of the local events was extracted from the *INGV Seismic Bulletin* [at

www.ingv.it/~roma/frames/frame-boll.html]. During 2002 the SAPTEX array reached its maximum configuration with up to 12 operating stations [additional details in *Cimini et al.*, 2005]. The seismic stations are the three-component Lennarz 5s sensors of the SAPTEX seismic experiment, the one-component S-13 sensors of the RSNC (with the exception of two stations; see Figure 2), and the three-component Lennarz Lite 1s sensors of the ENI-AGIP seismic network.

2.1. Hypocentral locations

Locations were computed with the HYPOELLIPSE code [*Lahr*, 1989] using the one-dimensional velocity model of *Chiarabba et al.* [2005]. We calculated an average Vp/Vs ratio equal to 1.82 using a modified Wadati method (Figure 3a). A well-constrained Vp/Vs ratio strongly helped in providing reliable hypocentral depth estimates.

A total of 204 events occurred between June 2001 and the end of 2002 within the study area and they have been relocated. The events have a magnitude Md ranging from 2.0 to 4.1 [*INGV Seismic Bulletin*] and their epicentral locations occur within a 260 km x 180 km area (within 15.0° E - 17.4° E and 39.8° N - 41.2° N).

From the collected seismograms, the arrival times of 2677 P and 1226 S phases were picked, giving a total of 3903 travel times. To provide some quantitative assessment of the reading uncertainty (s_{pick}) and hence determination of reasonable data weights ($1/s^2_{pick}$), we assigned a quality index to each arrival (Table 2). S phases are picked only on the three-component stations. Figure 3b shows the errors location, gap, residual values and phase numbers relative to the whole data set of events. We decided to rejected the earthquakes with horizontal (ERH) and vertical (ERZ) location errors larger than 1.5 and 2.2 km, respectively, and with azimuthal gaps larger than 195 degrees. The locations of the 120 remaining events are shown in Figure 4 and earthquake parameters are listed in Table 3. The average error on the horizontal direction is 0.25 km and on the vertical is 0.46 km (Table 3).

Based on the estimated hypocentral depths, most of the Lucanian region seismicity occurs within the upper crust, in the first 20 km. Only 17 out of the 120 detected events have hypocenters in the lower crust, ranging between 21 and 33 km. Six subcrustal earthquakes have been detected at depths between 37 and 92 km.

The analysis of the crustal seismicity indicates two regions with different pattern of earthquake epicentral distribution and depths (see Figure 4, vertical cross sections AB and CD). One region is centered along the axis of the Apenninic chain for a width of about 40 km, and the other includes the eastern outer margin of the chain and the foredeep.

The seismicity within the region of the Apenninic chain defines two main clusters. The northern one is limited at the Irpinia area and Pergola-Melandro basin, the second to the south in the upper Agri valley and the Castelluccio area. Within the latter, hypocenters are generally shallower with respect to the north, mostly occurring within the first 15 km of crust. Between these two areas, there is a strip of a 25 km-length along the axis of the chain where no shallow earthquakes (depth < 10 km, see shaded area in section EF in Figure 4) occurred during the investigated period; beneath this strip where the seismicity is completely absent, few events at the eastern border of the chain are spread at depths larger than 10 km (see cross-section EF in Figure 4). West of the chain, the crustal seismicity is almost absent (the Cilento area and the Policastro Gulf).

During the first two years of the SAPTEX deployment, a seismic sequence, named Savoia di Lucania in Table 3 and Figure 5a, was recorded at the north edge of the Pergola-Melandro basin (Figure 4). This sequence started with the April 18, 2002, Ml = 4.1, mainshock located at 11 km depth, followed by 24 aftershocks with magnitudes larger than 2.2 (Table 3). The aftershock epicenters show a cluster slightly elongated in a SW-NE direction (Figure 5a). Most of the hypocenters occur between 4 and 11 km and cluster at shallower depths with respect to the mainshock. The distribution of these events is concentrated within 2 km from the mainshock and delineates a sub-vertical "cloud" (Figure 5a). Few deeper events are spread below the mainshock. From the cross-sections in Figure 5a, we can infer that the rupture occurred along a sub-vertical plane, possibly with a SW-NE strike.

For the 25 events we obtain an average ERH=0.16 km with maximum value of 0.4 and an average ERZ=0.46 km with maximum of 1.2 km, belonging only to two events (see Table 3). The hypocentral locations of the Savoia di Lucania sequence evaluated in this study using the SAPTEX and RSNC network are substantially improved respect to those by *Cucci et al.* [2004], that report the maximum location errors of 1.9 km both for the horizontal coordinates and for the depths, with four events with larger vertical errors.

A significant swarm of 19 earthquakes, named Moliterno in Table 3 and Figure 5b, occurred along the S-SE side of the upper Agri valley in an area of 3 km x 5 km (Figure 4). It started on February 8, 2002 and lasted until December 2002 (end of the period investigated in this study). After four months of seismicity with ten events not larger than Md 2.8, there was a period of quiescence (June-September). Then, the seismic activity increased again starting from October 2002 with events closer in time and maximum magnitude of 3.2. Most of the hypocenters are concentrated at the depth interval between 3 km and 7 km (Figure 5b). The distribution of earthquakes does not fully constrain the fault-plane geometry, although a slight elongation of the epicenters in a WNW-ESE direction is observed (Figure 5b). Moreover, it is worth to note that this swarm is adjacent to the seismic sequence occurred in 1996 just to the northwest. A detailed analysis of the 1996 sequence has been carried out by *Cucci et al.* [2004], defining characteristics in terms of epicentral distribution, depths and magnitudes. These characteristics are very similar to those observed for the Moliterno swarm analyzed in this study.

Moving out from the region of the chain, we find changes in the pattern of crustal seismicity and define the second region at the eastern outer margin of the chain and in the foredeep (Figure 4). This region is characterized by broader and less frequent seismicity with deeper hypocenters ranging from 15 to 40 km (vertical cross sections AB and CD in Figure 4). Four isolated earthquakes locate within the foreland-foredeep, the Murge and Andria-Trani area (Figure 4), with depths larger than 20 km, except for the shallower Andria event. The only sequence recorded is located beneath the Bradano foredeep area. This sequence, named Basentano in Table 3 and Figure 4, consists of 5 events with depth ranging between 26 and 33 km, and maximum magnitude of 3.3 belonging to the westernmost event (Figure 4, vertical cross section CD). These few events do not allow us to constrain the geometry of the seismogenic structure.

At the northwestern sector of the study area, we observe a partial overlap of the shallow and deep crustal seismicity beneath the edge of the chain at depths between 15 and 25 km (Figure 4, vertical cross section AB). This overlap does not

occur to the south where the shallow and the deep hypocenters are adjacent but remain away from each other (Figure 4, vertical cross section CD).

Subcrustal earthquakes have also been recorded. Five of six have hypocenters ranging from 37 to 45 km depth. They are not clustered; four are located to the east of the chain (the lower Agri valley - 45 km, the lower Basentano valley - 38 km, the Murge Tarantine - 42 km, southeast of Potentino area - 42 km) and one is in the Lao valley - 41 km, close to the Tyrrhenian coast (Figure 4). A single 92 km-deep event was located within the Southern Tyrrhenian subduction zone nearby the Castelluccio area. This event reasonably belongs to the sparse seismicity that characterizes the northern edge of the subduction zone [depth range 50-150 km, *Frepoli et al.*, 1996].

2.2. Focal mechanisms computation

We computed best fit double-couple focal mechanisms using the fault-plane fit grid-search algorithm (FPFIT) of *Reasenberg and Oppenheimer* [1985]. We selected 34 out of 120 focal mechanisms (Figure 6 and Table 4) on the basis of quality factors Qf and Qp ranging from A to C for decreasing quality (Table 5). Qf reflects the solution prediction misfit of the polarity data Fj, while Qp reflects the solution uniqueness in terms of 90% confidence regions on strike, dip and rake. All solutions with one or both quality factor equal to C were rejected. Most of the fault-plane solutions shows more than 10 polarities (Table 4) and narrow azimuthal gap (<180°, see Table 3). We could compute and obtain constrained mechanisms even for events with magnitudes lower than 3.0, due to the dense seismic network.

Plunges of P- and T-axes were used to divide our data set into four main stress regime categories [*Zoback*, 1992]. Following this classification (see Table 4), 22 out of 34 focal mechanisms show prevalently normal fault solutions [16 are almost pure normal faulting (NF) and 6 have a minor strike-slip component (NS)], while 11 are almost pure strike-slip solutions (SS) and only one event shows a prevalent thrust fault mechanism with strike-slip component (TS, event 20 in Table 3). This thrust solution event occurs below the crust at 42 km of depth, and is located at the eastern outer margin of the chain (Figure 7). Most of the computed focal solutions belongs to the Apenninic chain sector (Figure 7), and are associated to events shallower than 20 km. Their T-axes are prevalently NE-SW oriented. Only seven out of 32 fault-plane solutions of crustal events show T-axis orientation ranging from NW-SE to E-W (events number 10, 51, 52, 91, 111, 114, 116 in Tables 3). The focal mechanism of the event at the intermediate depth of 92 km (number 87 in Table 3), which belongs to the northern portion of the Southern Tyrrhenian subduction zone, shows a P-axis plunge to the SW. We do not show the focal solutions relative to the events of the Savoia di Lucania sequence since they were not well constrained.

3. Fault-plane solution inversion for regional stress information

There is no correspondence between P- and T-axes of just a single fault-plane solution and the orientation of the maximum ($\sigma 1$) and minimum ($\sigma 3$) compressive stress directions [*McKenzie*, 1969]. The brittle shallow crust generally contains small preexisting faults of any orientation that may have low frictional coefficients. There is slip on these faults when a small component of the shear stress is resolved along the fault surface. In order to have a mechanical consistency

between the stress and the slip direction, the maximum ($\sigma 1$) and minimum ($\sigma 3$) compressive stress directions must be oriented somewhere within the dilatational and compressional quadrants, respectively, of the double-couple seismic radiation pattern.

All the developed inverse techniques used for finding the uniform stress field that is most consistent with a heterogeneous set of fault-plane solution data [*Angelier*, 1979, 1984; *Gephart and Forsyth*, 1984; *Michael*, 1984, 1985, 1987; *Gephart*, 1990a; *Rivera and Cisternas*, 1990] resolve four of the six parameters of the stress tensor. The unit vectors which define the orientation of the maximum ($\sigma 1$), intermediate ($\sigma 2$) and minimum ($\sigma 3$) compressive stress axis, and the factor shape $R= \sigma 2-\sigma 1/\sigma 3-\sigma 1$, which describes the relative magnitudes of the principal stresses. Thus factor shape R constrains the shape of the stress ellipsoid. The inverse techniques of focal solution data cannot determine the absolute magnitude of the deviatoric and isotropic stresses, but they only identify the best stress tensor model that most closely matches all the fault-plane solutions of the source region. The basic assumption is that the deviatoric stress tensor is uniform over the studied crust volume and during the investigated time interval. The focal mechanism stress inversion program (FMSI) of *Gephart*, [1990b] defines discrepancies between stress tensor orientation and observations by a misfit measure. The misfit of a single focal mechanism is defined as the minimum rotation about any arbitrary axis that brings one of the nodal planes and its slip direction into an orientation that is consistent with the slip direction predicted by a given stress model. The procedure uses a grid search technique operating in the whole space of stress parameters (stress directions and R). In this way the method finds the stress tensor that minimizes the average of misfits relative to all the fault-plane solutions.

We apply the *Gephart* [1990b] procedure to our data set of southern Italy fault-plane solutions of crustal earthquakes, with the purpose of investigating the stress field in the region at a greater level of detail than in the previous studies [e.g. *Montone et al.*, 2004; *Frepoli and Amato*, 2000a]. We assume a uniform stress field within the crust (2-25 km depth). The two focal mechanisms of the Basentano sequence (28 and 32 km of depth, respectively) were not considered for stress inversion because they are far away from the area where the most of the seismicity is concentrated (Figure 7). Because of variations in the quality of fault-plane solution estimates, we use a focal mechanism weighting scheme based on the quality factors described in the previous section "Focal mechanisms computation". Weights of 4 were assigned to (Qf, Qp) = (A, A) solutions, weights of 2 to (A, B) and (B, A) solutions, and weights of 1 to (B, B) solutions (Table 5). Larger weights provide more influence on the angular model misfit determinations. Moreover, an additional weight is given to the stronger events: 2 for events with magnitude equal or larger than 3.1.

Stress inversion with the 30 fault-plane solutions dataset (Figure 8a; the events selected are within the dashed black line in Figure 7) shows a nearly horizontal NE-SW minimum compressive stress axis ($\sigma 3$) (plunge 4°, trend 221°), while maximum compressive axis ($\sigma 1$) is quite oblique (plunge 54°, trend 317°). The R value of 0.4 indicates that the $\sigma 2$ amplitude lies almost in the middle of the range defined by $\sigma 1$ and $\sigma 3$. Minimum average misfit is quite large (7.5).

According to *Wyss et al.* [1992], average misfit values larger than 6.0 may be due to an inhomogeneous stress distribution within the considered crustal volume. For this reason, we perform two new inversions dividing the 30 events total dataset

into two sub-volumes (see the two dashed white lines in Figure 7): one to the north, including the Potentino-Irpinia-Savoia di Lucania area, with 18 focal mechanisms, and the other to the south, relative to the Moliterno swarm, with 11 events.

The results of the northern sector inversion (Figure 8b) show a stress orientation quite different from that of the whole dataset. The minimum compressive stress axis ($\sigma 3$) has plunge 12° and trend 93°, while the $\sigma 1$ is almost vertical with 75° of plunge and 312° of trend. The scalar R is 0.7 indicating that the intermediate compressive stress axis ($\sigma 2$) tends to be closer to the minimum axis ($\sigma 3$). The quite large misfit value (6.5) indicate a small heterogeneity inside the northern sector.

The Moliterno sub-volume inversion (Figure 8c) results comparable in the stress orientation, just slightly rotated toward north, with respect to that resulting from the inversion of the whole dataset (Figure 8a). The minimum compressive stress axis ($\sigma 3$) shows a 7° of plunge and a 206° of trend, while the maximum one ($\sigma 1$) has plunge 48° and trend 304°. The homogeneous tectonic regime (very small misfit) results from the inversion of focal mechanisms of the closely spaced events of the Moliterno swarm.

4. Discussion and Conclusions

In this paper we presented a detailed study of the seismicity occurred in the Lucanian region during the period June 2001-December 2002. We gathered the digital waveforms from two seismic networks: the RSNC and the temporary SAPTEX networks. To these data we added the P- and S- arrival times of the events recorded by the ENI-AGIP local network in the upper Agri Valley, to further improve earthquake location in that area. The resulting hypocentral locations are well constrained and reasonably improved with respect to those obtained by only RSNC data. This is due to the large amount of stations and to the closely spaced array used to locate the low magnitude seismicity of the Lucanian region.

During the observed period most of the seismicity was concentrated within the Apenninic chain (Figure 4). Conversely, at the eastern margin of the chain and in the Bradano foredeep the seismicity was very sparse. Seismicity defines two main clusters: the first is confined in the Irpinia area and in the Pergola-Melandro basin, the second to the south in the upper Agri valley and the Castelluccio area. Between these two areas, there is a region with a lack of shallow events and with only a few earthquakes occurring at depth larger than 10 km (see section EF in Figure 4). The western portion of the study region (Cilento and Policastro Gulf) is characterized by absence of crustal earthquakes. The spatial distribution of the earthquakes we have examined closely follows the pattern delineated by the seismicity of the last two decades (Figure 1). Then, despite the short time interval, the seismicity analyzed in this paper would be representative of the seismic behavior of the Lucanian region for such magnitudes even at longer order of time.

The relocated seismicity allow us to better discriminate the crustal regions characterized by shallow seismicity (within the first 20 km of depth) from those with deeper events (> 20 km depth) (see cross-sections in Figure 4). As general remark, seismicity deepens moving towards the external margin of the chain. Indeed, crossing the Lucanian region from SW to NE, we observe hypocentral depths that increase from about 20 km, along the chain, to about 30 km in the Bradano foredeep. Our results relative to the events in and around the area of the 1990 Potenza sequence (Potentino area) and to the events in

the Basentano area, whose hypocentral depths where in the range of 15 to 27 km and 26 to 33 km respectively (see Table 3), definitively stress that the outer margin of the Lucanian Apenninic chain and the Bradano foredeep area are characterized by deep crust seismicity. Within the external area and the foredeep, we also recorded four isolated subcrustal events (Figure 4).

Figure 9 shows the earthquake hypocenters located in the northwestern portion of the study area (section AB in Figure 4) superimposed to the geological-structural interpretation by *Merlini and Cippitelli* [2001] of a seismic line crossing the northern sector of the Vallo di Diano. The resulting section suggests that most of the upper crust earthquakes clusters in the brittle carbonate of the Apulian platform, and sparse events occur deeper in the basement as previously described; no background seismicity is apparently located in the shallower layers of the unit of the Lagonegro basin.

Fault-plane solutions are used to retrieve the stress tensor orientation. The stress inversion relative to the crustal earthquakes (Figure 8a) reveals that the Lucanian Apennine is generally ongoing through NE-SW extension, as the rest of the Apenninic chain [*Cucci et al.*, 2004; *Montone et al*., 2004; *Frepoli and Amato*, 2000a; *Pondrelli et al.*, 1998, among many others]. However, local heterogeneity in the stress orientation results from the fairly large average misfit, that were not previously identified.

In order to analyze this stress heterogeneity within the selected area (black dashed line in Figure 7), we subdivided the dataset and separately inverted the solutions belonging to the northern and the southern sectors of seismicity (white dashed lines in Figure 7). Concerning the northern sector, we obtain an almost E-W minimum compression stress axis ($\sigma 3$) and a small decreasing of the average misfit (Figure 8b). Despite the small amount of data and the relative large misfit, from this inversion it can be inferred a local rotation of the extensional axis in the area of the Vallo di Diano and Pergola-Melandro (Figures 4 and 7), from a regional NE-SW to an E-W direction.

The stress orientation of the southern sector of seismicity represents the local stress of the Moliterno swarm. For these swarm a small anticlockwise rotation of the minimum compressive axes ($\sigma 3$) is observed, being NNE-SSW oriented (Figure 8c) respect to the total inversion (Figure 8a). Thus, it can be extrapolate that NNE-SSW extension occurred inside the crustal volume of the Moliterno swarm.

Through the analysis of event locations we obtain some details about the source geometry of a sequence and a swarm occurred in the study period within the Lucanian chain. The spatial distribution of the Savoia di Lucania sequence well delineates a sub-vertical fault plane beneath the northern side of the Pergola-Melandro basin between 4 and 11 km of depth (Figure 5a). The observations on the earthquakes distribution and on the fault geometry are consistent with the hypothesis of a secondary fault bounding the northern tip of the NNW-SSE to NW-SE trending major seismogenic structure within the Pergola-Melandro basin [*Valensise and Pantosti*, 2001; *Moro et al.*, 2003; *Lucente et al.*, 2005]. The background seismicity such as that of the Savoia di Lucania sequence mostly develops at the border of the main NW-oriented fault segment [*Bisio et al.*, 2004; *Chiarabba et al.*, 2005].

The cross-sections of the Moliterno swarm shows a hardly perceptible high-dipping structure, between 3 and 7 km of depth. This swarm is located just to the ESE of that recorded in 1996 and analyzed by *Cucci et al.* [2004]. The NE-SW sections of this two upper Agri Valley sequences are quite similar in the fault plane geometry and suggests the presence,

along the southwestern side of the Valley, of a NW-SE to WNW-ESE oriented, ~NE dipping source that activated in two different period. The stress inversion relative to the Moliterno swarm indicates a NNE-SSW extensional regime (Figure 8c) that would be in agreement with the orientation of the inferred fault.

Our results stress out that in the Lucanian region there is eastward deepening of the hypocentral depths from inner to outer margin of the belt and foredeep (see cross sections in Figure 4) such as outlined by *Chiarabba et al.* [2005] for the external area of the northern and central Apennines system. The trend of the hypocentral depths delineated by the present study indicates a deeper boundary between the brittle and ductile crust beneath the external margin of the Lucanian Apennine and the foredeep, with respect to that beneath the chain itself. This different crustal setting is also suggested by tomographic and geothermal gradient studies that indicate for the outer and inland regions a brittle/ductile limit at 28-30 km and at 15-18 km, respectively [*Chiarabba and Amato*, 1996; *Harabaglia et al.*, 1997]. *Chiarabba et al.* [2005] report that the increasing of the seismogenic layer's depth follows the flexure of the Adria and Ionian lithosphere; despite the short period of detection, the pattern of deep crustal and subcrustal seismicity recorded in the eastern portion of the Lucanian region might be similarly interpreted.

Acknowledgment

We thank Eni-Agip for providing the P- and S- wave arrival times of the Agri Valley seismic network. We are grateful to Francesca Di Luccio for the suggestions and the fruitful comments to the work.

References

Amato, A., and G. Selvaggi (1993), Aftershock location and P-velocity structure in the epicentral region of the 1980 Irpinia earthquake, *Ann. di Geofis.*, *36*, (1), 3-25.

Angelier, J. (1979), Determination of the mean principal directions of stresses for a given fault population, *Tectonophysiscs*, *56*, T17-T26.

Angelier, J., (1984), Tectonic analysis of fault slip data sets, *J. Geophys. Res*., 89, 5835-5848.

Azzara, R., A. Basili, L. Beranzoli, C. Chiarabba, R. Di Giovambattista, and G. Selvaggi (1993), The seismic sequence of Potenza (May 1990), *Ann. Geofis*., *36* (1), 237-243.

Bisio, L., R. Di Giovambattista, G. Milano, and C. Chiarabba (2004), Three-dimensional earthquake locations and upper crustal structure of the Sannio-Matese region (southern Italy), *Tectonophysics*, *385*, 121–136.

Boschi, E., D. Pantosti, D. Slejko, M. Stucchi, and G. Valensise (1990), Irpinia dieci anni dopo, *Annali di Geofisica*, *36* (1), 169-351.

Castello B., Selvaggi G., Chiarabba C., Amato A., (2005), CSI Catalogo della sismicità italiana 1981-2002, versione 1.0. INGV-CNT, Roma, http://www.ingv.it/CSI/).

Chiarabba, C. and A. Amato (1996), Crustal velocity structure of the Apennines (Italy) from P-wave travel time tomography, *Ann. Geophys.*, *39* (6), 1133-1148.

Chiarabba, C., L. Jovane, and R. Di Stefano (2005), A new view of Italian seismicity using 20 years of instrumental recordings, *Tectonophysics*, *395*, 251-268.

Cimini G.B., P. De Gori, and A. Frepoli (2005), Passive seismology in southern Italy: the SAPTEX array, *Ann. Geophys.*, in press.

CPTI Working group (1999), Catalogo parametrico dei forti terremoti italiani, GNDT-ING-SGA-SSN (eds). *Editrice Compositori*, Bologna, 88 pp.

Cucci, L., S. Pondrelli, A. Frepoli, M.T. Mariucci, and M. Moro (2004), Local pattern of stress field and seismogenic sources in the Pergola-Melandro basin and the Agri Valley (Southern Italy), *Geoph. J. Int.*, *156* (3), 575-583.

Di Bucci, D., and S. Mazzoli (2003), The October-November 2002 Molise seismic sequence (southern Italy); an expression of Adria intraplate deformation, *J. of the Geol. Soc. of London*, *160* (4), 503-506.

Di Luccio, F., E. Fukuyama, and N.A. Pino (2005), The 2002 Molise earthquake sequence: what can we learn about the tectonics of Southern Italy?, *Tectonophysics*, submitted.

Ekstrom, G. (1994),Teleseismic analysis of the 1990 and 1991 earthquakes near Potenza, *Annali di Geofisica*, *37* (6), 1591-1599.

Frepoli, A., G. Selvaggi, C. Chiarabba, and A. Amato, (1996), State of stress in the Southern Tyrrhenian subduction zone from fault-plane solutions, *Geophys. J. Int.*, *125*, 879-891.

Frepoli, A., and A. Amato (2000a), Spatial variation in stresses in peninsular Italy and Sicily from background seismicity, *Tectonophysiscs*, *317*, 109-124.

Gephart, J. (1990a), Stress and the direction of slip on fault planes, *Tectonics*, *9*, 845-858.

Gephart, J. (1990b), FMSI: A FORTRAN program for inverting fault/slickenside and earthquake focal mechanism data to obtain the regional stress tensor, *Comput. Geosci.*, *16*, 953-989.

Gephart, J., and W. Forsyth (1984), An improved method for determining the regional stress tensor using earthquake focal mechanism data: Application to the San Fernando earthquake sequence, *J. Geophys. Res.*, *89*, 9305-9320.

Harabaglia, P., F. Mongelli, and G. Zito (1997), Geothermics of the Apenninic subduction, *Annali di Geofisica*, *40* (5), 1261-1274.

Lahr, J.C. (1989), HYPOELLIPSE/Version 2.0: A computer program for determining local earthquake hypocentral parameters, magnitude, and first motion pattern. *U.S. Geol. Surv. Open File Rep. 95*, 89-116.

Lucente F. P., N. Piana Agostinetti, M. Moro, G. Selvaggi, M. Di Bona (2005), Possible fault plane in a seismic gap area of the southern Apennines (Italy) revealed by receiver function analysis, *J. Geophys. Res.*, *110*, B04307, doi:10.1029/2004JB003187.

McKenzie, D.P. (1969), The relation between fault-plane solutions for earthquakes and the directions of the principal stresses, *Bull. Seismol. Soc. Am.*, *59* **(2)**, 591-601.

Merlini, S., and G. Cippitelli (2001), Structural styles inferred by seismic profiles, in Anatomy of an Orogen: the Apennines and adjacent Mediterranean Basins, G.B. Vai and I.P. Martini (eds.), *Kluwer Academic Publishers*, 441-454.

Michael, A. (1984), Determination of stress from slip data: Faults and folds, *J. Geophys. Res.*, *89*, 11517-11526.

Michael, A. (1985), Regional stress and large earthquakes: An observational study using focal mechanisms, Ph.D. thesis, Stanford Univ., Stanford, California.

Michael, A. (1987), Use of focal mechanisms to determine stress: A control study, *J. Geophys. Res.*, *92*, 357-368.

Michetti, A.M., L. Ferrelli, E. Esposito, E. Porfido, A.M. Blumetti, E. Vittori, L. Serva, and G.P. Roberts (2000), Ground effects during the 9 september 1998, Mw = 5.6, Lauria earthquake and the seismic potential of the "aseismic" Pollino region in Southern Italy, *Seimological Research Letters*, *41* (1), 31-46.

Montone, P., M.T. Mariucci, S. Pondrelli, and A. Amato (2004), An improved stress map for Italy and surrounding regions (Central Mediterranean), *J. Geophys. Res.*, *109*, B10410, doi: 10.1029/2003JB002703.

Moro, M., L. Amicucci, F.R. Cinti, F. Doumaz, P. Montone, S. Pierdominici, and M. Saroli (2003), Evidence for Late Pleistocene-Holocene Activity along a Potential Seismic Source in southern Apennines (Italy), *Eos Trans. AGU*, *84*(46), Fall Meet. Suppl., T51D-0199.

Pondrelli, S., A. Morelli, and G. Ekström (1998), Moment tensors and seismotectonics of the Mediterranean region, *Ann. Geophys*., 16 suppl., C19.

Pondrelli, S., A. Morelli, G. Ekström, S. Mazza, E. Boschi, and A.M. Dziewonski (2002), European-Mediterranean regional centroid-moment tensors: 1997-2000, *Phys. Earth Planet. Int.*, *130*, 71-101. (Quick Regional CMT available at: http://mednet.ingv.it/events/QRCMT/Welcome.html)

Rivera, L., and A. Cisternas (1990), Stress tensor and fault-plane solutions for a population of earthquakes, *Bull. Seismol. Soc. Am*., *80*, 600-614.

Reasenberg, P., and D. Oppenheimer (1985), FPFIT, FPPLOT and FPPAGE: FORTRAN computer programs for calculating and displaying earthquake fault-plane solutions, *U.S. Geol. Surv. Open-File Rep.* 85-739.

Valensise, G., and D. Pantosti (2001), eds. Database of potential sources for earthquakes larger than M 5.5 in Italy, *Suppl. to Ann. Geofis.*, *44*, 4, 797-964.

Valensise, G., D. Pantosti, and R. Basili (2004), Seismology and Tectonic Setting of the 2002 Molise, Italy, Earthquake *Earthquake Spectra*, *20*, S23.

Wyss, M., Liang, B., W.R. Tanigawa, and X. Wu (1992), Comparison of orientations of stress and strain tensors based on fault-plane solutions in Kaoiki, Hawaii, *J. Geophys. Res.*, *97*, 4769-4790.

Zoback, M.L. (1992), First- and second-order patterns of stress in the lithosphere: The World Stress Map Project. *J. Geophys. Res*., *97 B8*, 11703-11728.

Table 1. Parameters of the largest instrumental earthquakes in the southern Apennines (parameters of the Irpinia event are from *Amato and Selvaggi* [1993], of the two Potenza earthquakes are from *Ekstrom* [1994], of the Castelluccio-Lauria are from Harvard CMT Catalogue). The CMT (Centroid Moment Tensor) solutions of these earthquakes are shown in Figure 1, except for the unavailable mechanism of event nr. 3.

Nr.	Epicenter	Date	Latitude °N	Longitude °E	Mw	Depth (km)
1	Irpinia	11/23/1980	40.724	15.373	6.9	10
2	Potenza	05/05/1990	40.775	15.766	5.7	9-13
3	Potenza	05/26/1991	40.730	15.765	5.2	11
4	Castelluccio-Lauria	09/09/1998	40.015	15.947	5.6	10

Table 2. Picking accuracy quality index assigned to each P- and S- arrival.

a quality	**b** quality	**c** quality	**d** quality
0.04 s (1879 picks)	0.10 s (753 picks)	0.20 s (621 picks)	0.40 s (650 picks)

Table 3. Hypocentral parameters, duration magnitude, azimuthal gap, location errors (rms, ERH, ERZ), total number of P and S phases used for location, location quality and geographic area of the 120 earthquakes selected in this study.

N.	Date (yr/m/day)	O.T. (h/min.)	Latitude °N	Longit. °E	Depth (km)	Md	Gap	Rms (sec)	ERH (km)	ERZ (km)	Number of P and S phases	Q	Region
1	010708	09:49	40.7567	15.4363	12.7	2.4	162	0.11	0.4	0.3	7	A	Irpinia
2	010725	09:22	39.9993	16.0058	10.7	2.3	125	0.03	0.9	1.4	7	B	Castelsaraceno
3	010728	05:05	40.8722	15.3398	9.5	2.2	166	0.03	0.2	0.3	9	A	Irpinia
4	010812	09:12	40.805	15.2282	12.1	2.6	124	0.04	0.3	0.7	9	A	Irpinia
5	010814	00:55	40.7958	15.3055	11.2	3.0	86	0.41	0.1	0.2	35	A	Irpinia
6	010817	01:45	40.6832	15.5205	11.6	2.5	109	0.05	0.4	0.4	10	A	Irpinia
7	010820	06:01	40.4325	15.576	1.7	3.3	58	0.47	0.1	0.1	24	A	Vallo di Diano
8[a]	010914	08:02	40.6382	15.7203	24.5	2.8	98	0.19	0.2	0.2	30	A	Potentino
9	010917	21:04	40.9703	15.0873	14.7	2.3	156	0.01	0.5	0.9	4	A	Irpinia
10[a]	010930	23:44	40.223	16.04	12.6	2.7	111	0.34	0.1	0.1	28	A	S. Martino d'Agri
11	011007	08:38	40.509	15.626	14.4	2.3	187	0.01	0.4	0.5	6	A	Brienza
12	011008	14:42	40.4967	15.3997	13.8	2.2	150	0.06	0.9	1.4	5	B	Alburni Mts
13[a]	011013	18:57	40.45	15.652	18.6	2.2	187	0.18	0.2	0.3	10	A	Brienza
14	011013	23:32	40.7493	15.3862	14.1	2.2	153	0.06	1.2	1.8	5	B	Irpinia
15	011023	11:05	40.8427	15.1617	18.1	2.3	137	0.01	0.6	1.4	6	B	Irpinia
16	011027	12:09	41.2147	16.298	4.9	2.7	146	0.11	06	0.4	19	A	Andria
17[a]	011104	10:22	40.4313	16.1243	16.8	2.5	75	0.38	0.1	0.2	29	A	Stigliano
18[a]	011104	10:28	40.434	16.1197	16.6	3.0	53	0.42	0.1	0.2	41	A	Stigliano
19	011104	23:49	40.4858	15.596	9.9	2.4	58	0.34	0.1	0.1	31	A	Brienza
20[a]	011113	13:21	40.53	15.942	41.8	2.4	45	0.60	0.1	0.2	38	A	Central Lucania
21	011121	06:10	40.5127	15.8157	18.4	2.8	77	0.24	0.1	0.2	27	A	Calvello
22[a]	011121	06:21	40.5217	15.8213	18.1	2.7	94	0.22	0.1	0.2	26	A	Calvello
23[a]	011209	12:15	40.7722	15.275	12.1	3.2	96	0.30	0.1	0.2	29	A	Irpinia
24	011213	04:33	40.746	15.264	17.4	2.3	144	0.01	0.4	1.0	5	A	Irpinia
25	011219	06:36	39.8865	15.5945	3.4	2.7	166	0.38	0.3	0.4	14	A	Policastro gulf
26[a]	020102	02:09	40.753	15.392	11.6	2.7	82	0.28	0.1	0.2	19	A	Irpinia
27[a]	020102	02:17	40.7608	15.3995	12.8	2.8	80	0.27	0.1	0.2	32	A	Irpinia
28	020114	01:47	40.183	15.6547	9.7	2.5	151	0.15	0.2	0.5	11	A	Morigerati
29[a]	020115	00:06	40.7982	15.7622	22.2	2.6	155	0.32	0.1	0.4	24	A	Potentino
30	020115	00:11	40.7913	15.7828	16.0	2.6	151	0.20	0.2	0.8	14	A	Potentino
31	020115	01:29	40.836	15.7505	26.7	2.4	122	0.48	0.3	0.9	18	A	Potentino
32	020122	12:43	40.5578	15.606	10.7	2.6	114	0.15	0.2	0.2	20	A	Savoia di Lucania
33	020130	19:42	40.8	16.6382	21.3	2.0	124	0.16	0.1	0.5	16	A	Murge
34[a]	020208	04:38	40.2418	15.913	3.7	2.6	47	0.32	0.1	0.3	22	A	Moliterno
35	020211	21:09	40.8288	15.3283	16.2	2.5	153	0.25	0.3	0.4	23	A	Irpinia
36	020213	04:20	39.8305	15.8973	40.6	2.6	126	0.34	0.4	0.3	18	A	Lao Valley
37	020214	02:34	40.7403	15.6427	20.1	2.6	160	0.08	0.3	0.9	12	A	Potentino
38[a]	020226	17:12	40.2278	15.9193	4.6	2.6	95	0.19	0.1	0.1	29	A	Moliterno
39	020303	18:30	40.539	15.536	11.7	2.1	163	0.12	0.5	2.1	6	B	Savoia di Lucania
40	020304	00:44	40.7528	15.6788	14.6	2.4	129	0.16	0.3	0.9	12	A	Potentino
41	020316	02:01	40.5803	15.288	3.0	2.2	112	0.26	0.2	0.1	8	A	Alburni Mts
42[a]	020317	04:53	40.2335	15.9135	3.0	2.8	53	0.37	0.1	0.3	18	A	Moliterno
43	020317	06:09	40.231	15.8257	11.5	2.5	83	0.26	0.3	1.8	8	B	Moliterno
44	020320	17:34	40.7257	15.2443	7.1	2.4	116	0.16	0.3	1.8	11	B	Irpinia
45	020324	00:11	40.2408	16.4877	45.5	2.8	153	0.47	0.2	0.2	27	A	Lower Agri Valley
46	020328	09:59	40.34	17.361	41.6	2.8	139	0.19	0.4	1.9	13	B	Murge Tarantine
47	020402	04:22	40.246	15.863	4.1	2.7	56	0.56	0.1	0.2	27	A	Moliterno

48	020404	22:07	40.5068	15.806	10.2	2.3	113	0.31	0.3	0.8	23	A	Brienza
49[a]	020413	08:44	40.5112	15.8043	16.4	2.7	68	0.22	0.1	0.2	35	A	Calvello
50[a]	020413	10:48	40.1728	15.9105	4.7	2.5	66	0.24	0.1	0.2	31	A	Moliterno
51[a]	020413	17:04	40.5635	16.4205	28.0	3.3	70	0.36	0.1	0.1	47	A	Basentano
52[a]	020413	17:16	40.4965	16.4173	32.4	2.4	100	0.25	0.2	0.1	37	A	Basentano
53	020413	19:52	40.5875	16.4397	27.2	2.2	117	0.20	0.5	0.9	18	A	Basentano
54	020413	20:28	40.5452	16.4855	33.3	2.5	106	0.25	0.3	0.1	21	A	Basentano
55	020413	20:31	40.5717	16.469	26.4	2.6	99	0.11	0.2	0.5	20	A	Basentano
56	020418	20:56	40.5738	15.5463	11.1	4.1[b]	54	0.30	0.1	0.1	46	A	Savoia di Lucania
57	020418	20:58	40.595	15.5697	9.2	2.8	115	0.37	0.1	0.2	23	A	Savoia di Lucania
58	020418	21:00	40.5723	15.5452	8.5	3.2	55	0.37	0.1	0.2	37	A	Savoia di Lucania
59	020418	21:36	40.567	15.5512	7.0	3.1	68	0.32	0.1	0.3	34	A	Savoia di Lucania
60	020418	21:37	40.5778	15.558	5.6	2.7	110	0.40	0.1	0.2	27	A	Savoia di Lucania
61[a]	020418	22:58	40.5698	15.5485	5.6	3.0	55	0.37	0.1	0.2	36	A	Savoia di Lucania
62	020418	23:19	40.5725	15.5545	9.8	3.1	54	0.32	0.1	0.2	37	A	Savoia di Lucania
63	020418	23:56	40.6173	15.4867	12.3	2.2	113	0.23	0.4	0.4	11	A	Savoia di Lucania
64	020419	22:12	40.5783	15.545	8.8	2.6	93	0.31	0.2	1.1	13	B	Savoia di Lucania
65	020420	20:37	40.5943	15.5578	1.5	2.3	114	0.21	0.1	0.3	12	A	Savoia di Lucania
66	020420	23:31	40.5815	15.556	5.5	2.6	96	0.24	0.2	0.2	26	A	Savoia di Lucania
67	020421	00:57	40.5737	15.5197	9.0	3.1	75	0.48	0.1	0.2	36	A	Savoia di Lucania
68	020421	01:01	40.5918	15.5333	18.5	2.6	111	0.06	0.3	0.9	9	A	Savoia di Lucania
69	020421	23:39	40.573	15.5418	5.1	3.5	60	0.33	0.1	0.1	50	A	Savoia di Lucania
70	020423	15:58	40.2545	15.883	11.2	2.4	54	0.29	0.1	0.2	30	A	Moliterno
71	020423	21:14	40.6073	15.4977	22.3	2.4	104	0.04	0.3	1.2	9	A	Savoia di Lucania
72	020425	15:06	40.2578	16.4288	16.9	2.4	155	0.28	0.3	0.2	33	A	Lower Agri Valley
73	020426	19:14	40.2388	15.8745	4.9	2.3	66	0.17	0.1	0.1	28	A	Moliterno
74	020429	03:19	40.561	15.5443	5.6	3.2	56	0.31	0.1	1.2	32	B	Savoia di Lucania
75	020429	19:23	40.4337	16.2103	16.7	2.8	89	0.25	0.1	0.3	32	A	Stigliano
76[a]	020504	09:41	40.6617	15.507	16.6	2.7	62	0.24	0.1	0.2	35	A	Irpinia
77	020505	06:40	40.6067	15.6013	23.5	2.4	57	0.15	0.1	0.2	30	A	Savoia di Lucania
78	020508	19:29	40.0662	15.9725	9.8	3.1	62	0.37	0.1	0.3	37	A	Castelluccio
79	020508	20:46	40.0413	16.2057	13.0	2.6	78	0.35	0.2	0.2	35	A	Francavilla in Sinni
80	020508	22:36	40.0488	16.2392	24.2	2.5	80	0.45	0.1	0.3	33	A	Francavilla in Sinni
81	020509	23:55	40.3832	16.5958	37.7	2.5	155	0.24	0.1	0.3	34	A	Lower Basentano
82[a]	020512	20:20	40.652	15.7577	22.0	2.6	141	0.30	0.1	0.2	35	A	Potentino
83	020518	19:04	40.5645	15.5023	17.7	2.4	107	0.14	0.2	0.6	10	A	Savoia di Lucania
84	020526	08:46	40.5283	15.473	10.2	2.2	113	0.06	0.3	1.1	8	A	Savoia di Lucania
85	020526	10:19	40.5423	15.4993	10.0	2.6	103	0.27	0.1	0.3	25	A	Savoia di Lucania
86	020531	16:31	40.2243	15.8955	2.6	2.8	57	0.24	0.1	0.2	34	A	Moliterno
87[a]	020607	05:47	39.9655	16.0048	91.8	2.2	105	0.58	0.2	0.5	28	A	Castelluccio
88	020608	23:04	40.571	15.4717	14.5	2.4	93	0.30	0.1	0.3	24	A	Savoia di Lucania
89	020609	09:27	40.2152	15.9237	3.9	2.3	76	0.32	0.1	0.2	25	A	Moliterno
90[a]	020611	20:02	40.5093	15.6928	15.5	3.1	57	0.41	0.1	0.1	45	A	Brienza
91[a]	020618	23:31	40.5272	15.7308	13.0	2.7	51	0.36	0.1	0.1	36	A	Calvello
92	020623	21:41	41.2488	16.3867	22.4	2.8	158	0.19	0.2	0.4	26	A	Trani
93	020708	08:12	40.703	15.259	18.4	2.5	153	0.10	0.6	1.6	14	B	Irpinia
94	020711	03:36	39.873	15.9877	5.3	2.3	132	0.59	0.1	0.4	14	A	Castelluccio
95	020713	11:49	39.9773	16.0587	5.7	2.9	87	0.21	0.1	1.0	31	A	Castelluccio
96	020717	21:48	40.6725	15.5975	3.6	2.6	158	0.35	0.3	0.7	9	A	Irpinia
97	020718	08:23	39.9467	16.0268	25.0	2.8	102	0.57	0.1	0.3	24	A	Castelluccio
98[a]	020718	08:28	39.974	16.0582	2.3	2.8	88	0.27	0.1	0.3	24	A	Castelluccio
99	020721	22:50	40.7392	15.2955	12.7	2.6	139	0.20	0.6	0.7	13	A	Irpinia
100	020809	06:16	40.5622	15.4907	3.8	2.7	137	0.44	0.2	0.4	19	A	Savoia di Lucania
101	020810	23:04	40.7868	15.3587	5.4	2.7	119	0.20	0.2	0.4	10	A	Irpinia
102	020824	06:43	40.6307	15.7685	22.9	2.1	142	0.20	0.2	0.2	29	A	Potentino
103	020901	06:43	40.694	15.6412	4.0	2.3	103	0.61	0.2	0.7	19	A	Irpinia
104[a]	020903	01:45	40.4972	15.6535	16.8	2.5	78	0.23	0.1	0.1	36	A	Brienza
105	020920	07:35	40.6642	15.8308	25.2	2.7	63	0.20	0.1	0.2	38	A	Potentino
106	020930	04:24	40.0242	15.6265	4.6	2.5	193	0.18	0.2	0.3	28	A	Policastro gulf
107	021003	22:56	40.2245	15.93	5.7	2.5	61	0.23	0.1	0.1	34	A	Moliterno
108[a]	021004	22:58	40.2353	15.9233	5.4	3.2	52	0.34	0.1	0.1	46	A	Moliterno
109[a]	021006	02:43	40.2252	15.9195	5.9	2.3	60	0.25	0.1	0.1	35	A	Moliterno
110	021008	18:26	40.5955	15.4873	11.0	2.4	95	0.52	0.1	0.5	26	A	Savoia di Lucania
111[a]	021017	15:19	40.3975	15.7673	15.2	2.1	64	0.19	0.1	0.2	26	A	Marsico Vetere
112	021106	20:07	40.574	15.554	6.9	2.3	108	0.35	0.1	0.4	26	A	Savoia di Lucania
113[a]	021109	01:53	40.8077	15.8412	18.6	2.5	87	0.23	0.1	0.3	21	A	Potentino
114[a]	021119	16:53	40.2268	15.9173	4.8	2.2	79	0.22	0.1	0.2	32	A	Moliterno
115	021125	22:51	40.5935	15.5648	10.2	2.5	116	0.24	0.2	0.6	23	A	Savoia di Lucania
116[a]	021129	10:54	40.2158	15.9057	4.9	2.3	82	0.25	0.1	0.2	30	A	Moliterno
117[a]	021130	01:19	40.2175	15.8975	4.2	2.8	82	0.25	0.1	0.2	30	A	Moliterno
118[a]	021130	17:33	40.2162	15.9083	5.1	2.7	56	0.19	0.1	0.1	32	A	Moliterno
119	021201	00:30	40.214	15.9197	6.7	2.5	62	0.17	0.1	0.3	30	A	Moliterno
120	021228	00:22	40.2235	15.9233	4.4	2.2	61	0.14	0.1	0.2	31	A	Moliterno

[a] events with fault-plane solutions (see Table 4)

[b] local magnitude (Ml)

Table 4. Parameters of the computed fault-plane solutions. Event numbers correspond to those in Table 3. It is reported the strike, dip and rake of one of the two nodal planes, number of polarities, quality factor (Qf, Qp, see also Table 5) and stress regime categories (Fps): normal faulting (NF), predominately normal with strike-slip component (NS), strike-slip faulting (SS) and predominately thrust with strike-slip component (TS).

N.	Date	O.T.	Strike	Dip	Rake	N. Pol.	Qf	Qp	Fps
8	010914	08:02	95	50	160	10	A	A	SS
10	010930	23:44	30	70	-80	14	A	A	NF
13	011013	18:57	155	10	-60	7	A	B	NF
17	011104	10:22	120	20	-140	11	A	A	NF
18	011104	10:28	130	20	-90	16	B	A	NF
20	011113	13:21	130	60	150	13	A	B	TS
22	011121	06:21	115	30	-130	12	A	A	NF
23	011209	12:15	125	50	-90	16	B	A	NF
26	020102	02:09	145	25	-80	6	A	A	NF
27	020102	02:17	105	70	-90	10	B	A	NF
29	020115	00:06	285	80	-140	8	A	A	SS
34	020208	04:38	135	15	-80	11	B	A	NF
38	020226	17:12	165	30	-70	10	A	B	NF
42	020317	04:53	110	25	-140	10	B	A	NF
49	020413	08:44	25	85	-20	13	A	B	SS
50	020413	10:48	285	75	-150	8	A	B	SS
51	020413	17:04	345	70	-140	25	B	A	NS
52	020413	17:16	20	35	-80	11	B	A	NF
61	020418	22:58	290	75	-160	12	A	B	SS
76	020504	09:41	145	25	-80	11	B	B	NF
82	020512	20:20	295	90	180	12	A	A	SS
87	020607	05:47	275	70	0	11	B	A	SS
90	020611	20:02	5	55	-60	18	B	A	NF
91	020618	23:31	340	90	-170	19	A	A	SS
98	020718	08:28	280	60	-120	9	A	A	NF
104	020903	01:45	80	60	-140	16	B	A	NS
108	021004	22:58	320	80	-20	18	A	A	SS
109	021006	02:43	85	70	-140	12	B	A	NS
111	021017	15:19	40	15	-70	11	B	B	NF
113	021109	01:53	85	50	-150	8	A	A	NS
114	021119	16:53	50	50	-10	10	A	A	SS
116	021129	10:54	145	70	-130	9	A	A	NS
117	021130	01:19	255	70	-160	14	A	A	SS
118	021130	17:33	115	70	-140	13	B	A	NS

Table 5. Fault-plane solution quality factors Qf and Qp. Fj is the solution prediction misfit to the polarity data; Δstr, Δdip, Δrake are ranges of variability of strike, dip and rake, respectively.

	Qf		Qp
A	$Fj \leq 0.025$	A	$\Delta str, \Delta dip, \Delta rake \leq 20°$
B	$0.025 < Fj \leq 0.1$	B	20° to 40°
C	$Fj > 0.1$	C	> 40°

Figures Captions

Figure 1. Seismicity map of southern Italy [*Castello et al.*, 2005; *INGV Seismic Bulletin*; *CPTI Working group*, 1999] from 1981 to present. The dates of occurrence for the largest events are indicated. The available CMT (Centroid Moment Tensor) solutions of the earthquakes of M = 5.0 are also shown [*Pondrelli et al.*, 2002]. Numbered focal spheres correspond to events in Table 1.

Figure 2. Map of seismic stations used in this study. White triangles are the three-components permanent stations of the Italian National Seismic Network (RSNC), white square are the three-components temporary stations of the SAPTEX array, white stars are the short-period three-components stations of the ENI-AGIP local network in the Agri Valley area and dark-grey triangles are the one-component stations of the RSNC.

Figure 3. (a) Wadati diagram for all the events analyzed reporting the differences between P and S arrivals for each couple of station. The double differences are fitted by a linear regression. The slope of the right line is the Vp/Vs ratio; (b) final location rms, horizontal and vertical errors, azimuthal gap for the locations of the whole data set, histograms of P-wave and S-wave residuals and events frequency with phases number of the whole data set.

Figure 4. Epicentral locations, depths and magnitudes of the local seismicity (120 earthquakes) selected for this study in the Lucanian region. The three cross-sections in the insets show the projection of the hypocenters (see locations in the map). The maximum earthquake distance from sections AB, CD and EF is 30 km, 50 km and 200 km, respectively. Topography is vertically exaggerated.

Figure 5. Epicentral locations and depth distribution of the (a) Savoia di Lucania and (b) Moliterno seismic sequences. Star indicates the mainshock hypocenter of the Savoia di Lucania sequence. Topography is vertically exaggerated.

Figure 6. Focal mechanisms computed with first motion polarities for 34 selected events. Event number corresponds to that in Table 3.

Figure 7. Map showing the distribution of the 34 selected fault-plane solutions. Focal mechanisms in grey belongs to the subcrustal events. Duration magnitude and event number of Table 3 and Table 4 are shown close to each fault-plane solution. Black dashed line encircle the crustal volume considered for the total stress inversion, while the two white dashed lines encircle the two sub-volumes considered for the further stress inversions (see text for explanation).

Figure 8. Stress inversion results using: (a) 30 solutions; (b) 18 solutions within the northern sector (Irpinia-Potentino-Savoia di L.-Calvello); (c) 11 solutions of earthquakes within the southern sector (Moliterno-S. Martino d'Agri). For the location of the two sectors see Figure 7. For each inversion is shown the stereonet plot with the 95% confidence limits for $\sigma 1$ (small crosses) and $\sigma 3$ (small squares) and the histogram illustrating the uncertainity in the parameter R. Plunge and trend for the three principal stress axes are shown below the histograms.

Figure 9. Crustal and subcrustal seismicity (section AB in Figure 4) superimposed on the geological and structural interpretation of a NE-SW oriented seismic line [modified by *Merlini and Cippitelli*, 2001].

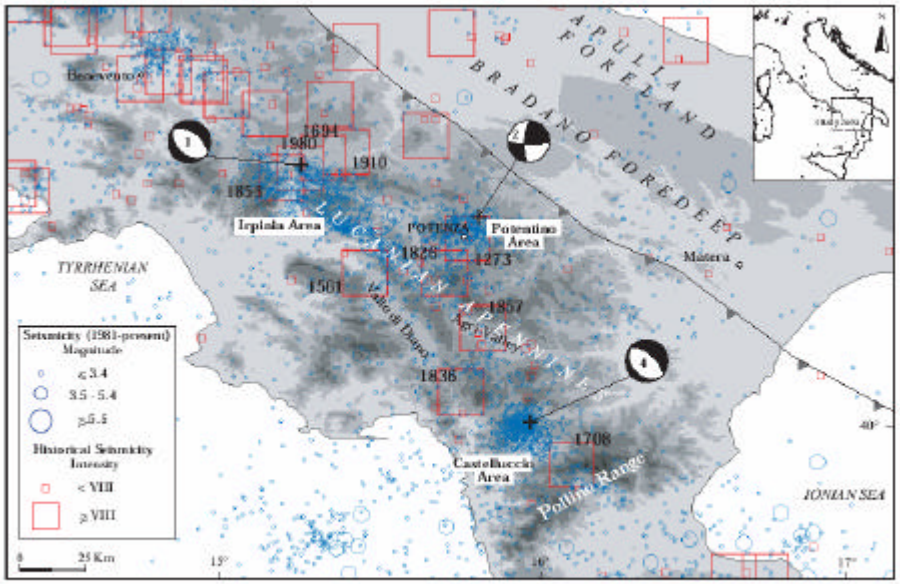

FIGURE 1

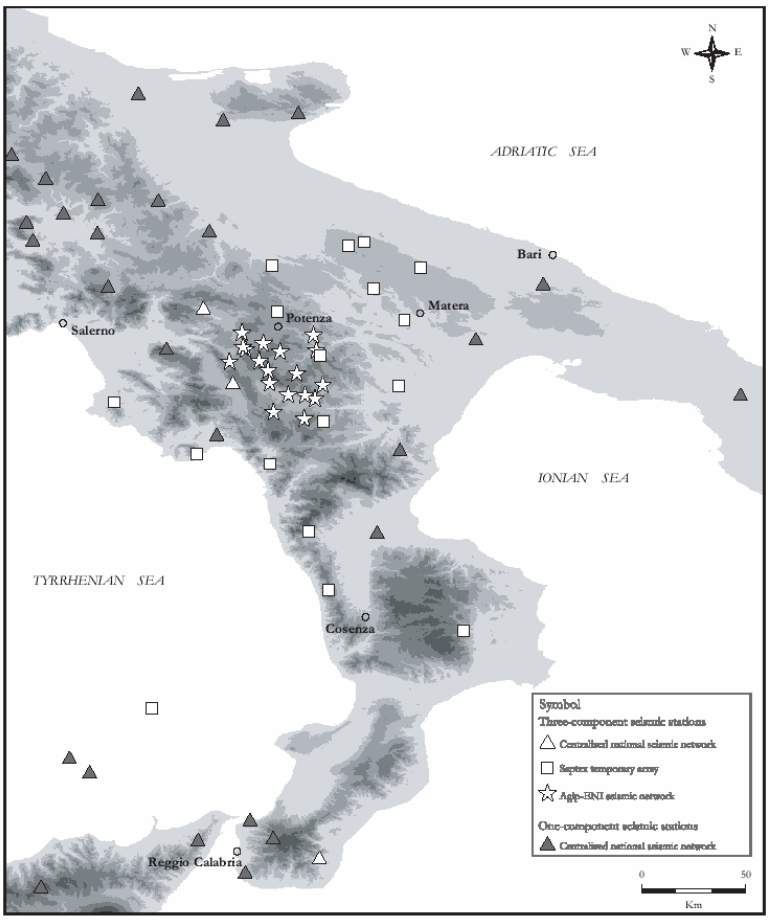

FIGURE 2

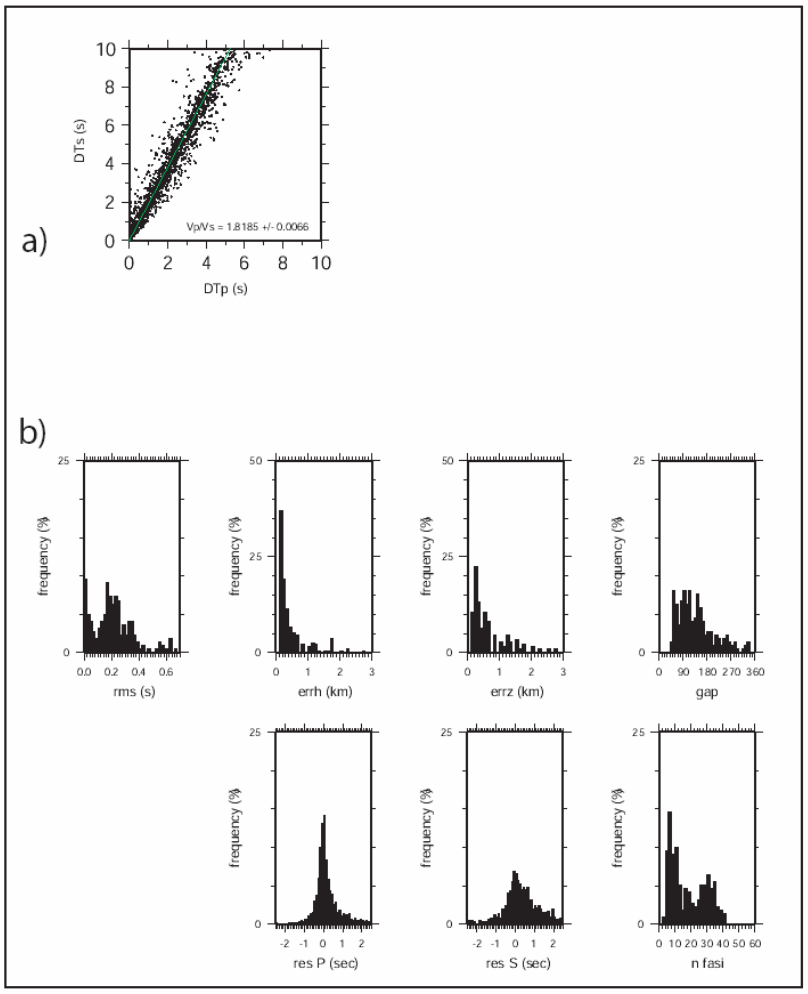
a)
DTs (s)
DTp (s)
Vp/Vs = 1.8185 +/- 0.0066
b)
frequency (%)
rms (s)
errh (km)
errz (km)
gap
res P (sec)
res S (sec)
n fasi

FIGURE 3

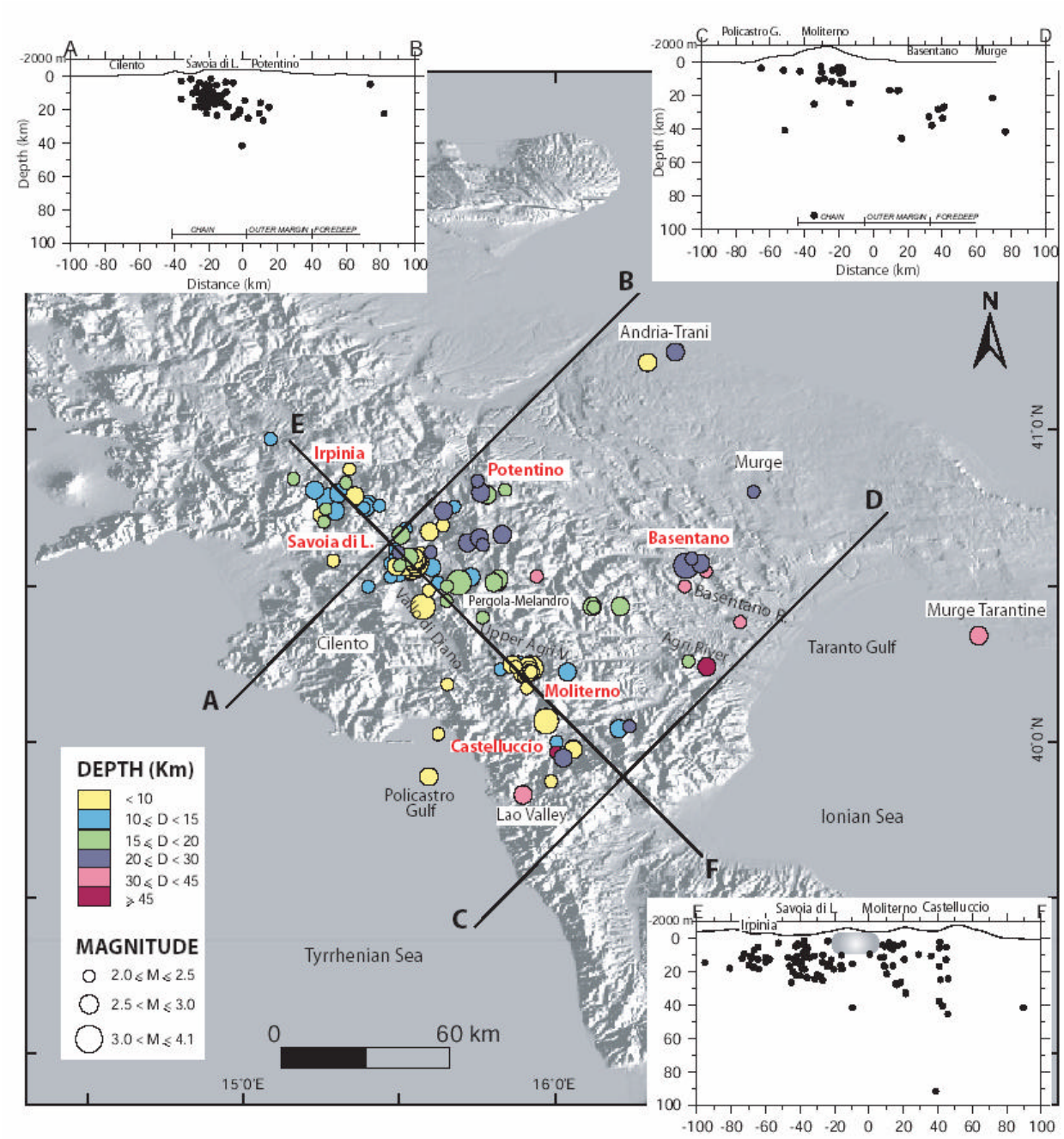
A
B
C
D
E
F
Cilento
Savoia di L.
Potentino
Depth (km)
Distance (km)
CHAIN
OUTER MARGIN
FOREDEEP
Policastro G.
Moliterno
Basentano
Murge
Irpinia
Moliterno Castelluccio
Andria-Trani
Pergola-Melandro
Upper Agri V.
Agri River
Basentano R.
Murge Tarantine
Taranto Gulf
Ionian Sea
Tyrrhenian Sea
Policastro Gulf
Lao Valley
Lago di Pano
N
41°0'N
40°0'N
15°0'E
16°0'E
0
60 km
DEPTH (Km)
< 10
10 ≤ D < 15
15 ≤ D < 20
20 ≤ D < 30
30 ≤ D < 45
≥ 45
MAGNITUDE
2.0 ≤ M ≤ 2.5
2.5 < M ≤ 3.0
3.0 < M ≤ 4.1

FIGURE 4

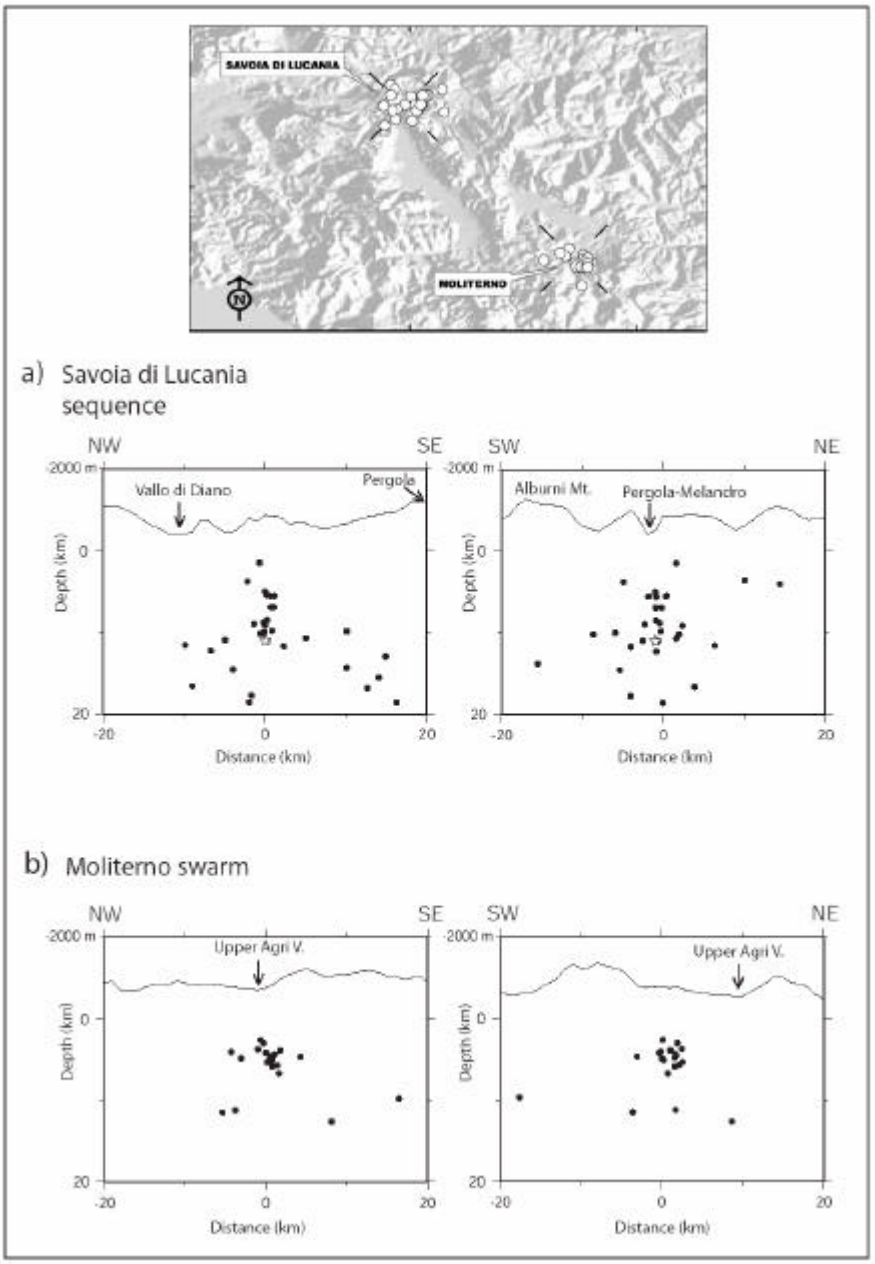
SAVOIA DI LUCANIA
MOLITERNO
a) Savoia di Lucania sequence
NW
SE
SW
NE
-2000 m
Vallo di Diano
Pergola
Alburni Mt.
Pergola-Melandro
Depth (km)
0
20
-20
Distance (km)
b) Moliterno swarm
Upper Agri V.

FIGURE 5

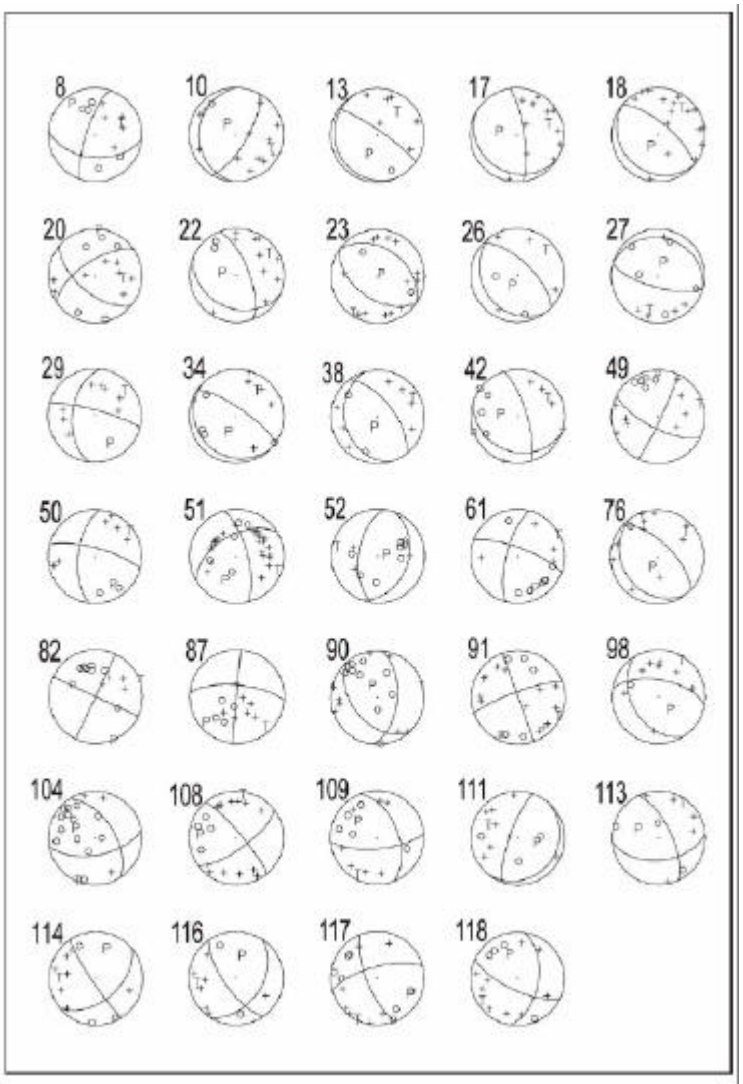
8
10
13
17
18
20
22
23
26
27
29
34
38
42
49
50
51
52
61
76
82
87
90
91
98
104
108
109
111
113
114
116
117
118

FIGURE 6

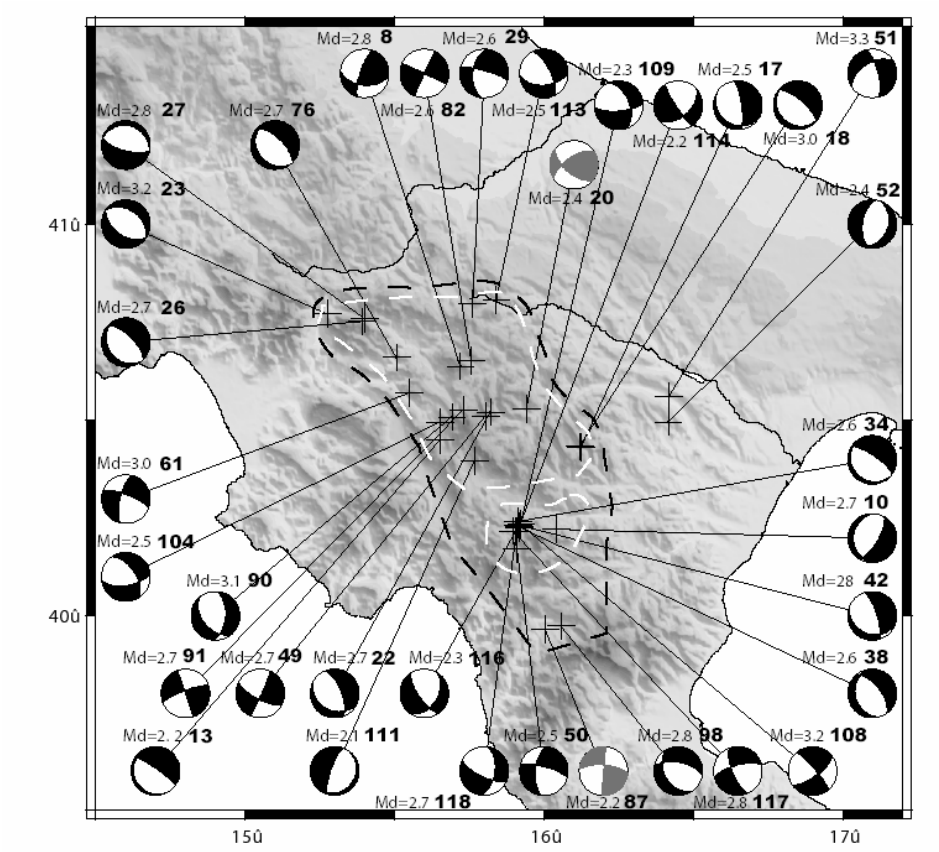

FIGURE 7

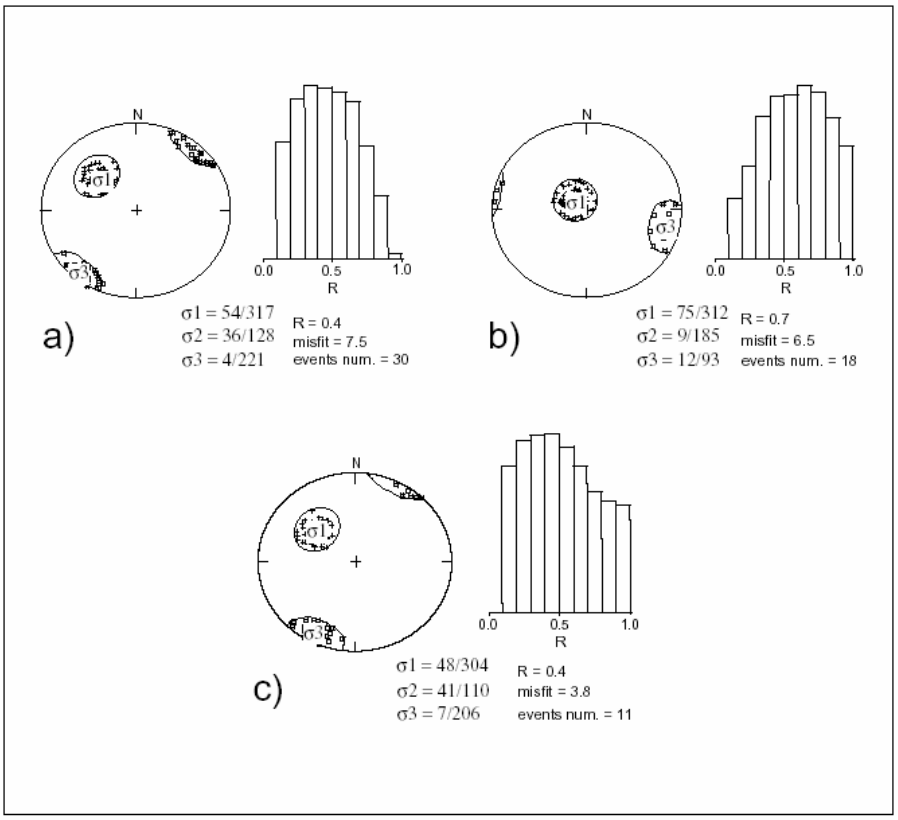

FIGURE 8

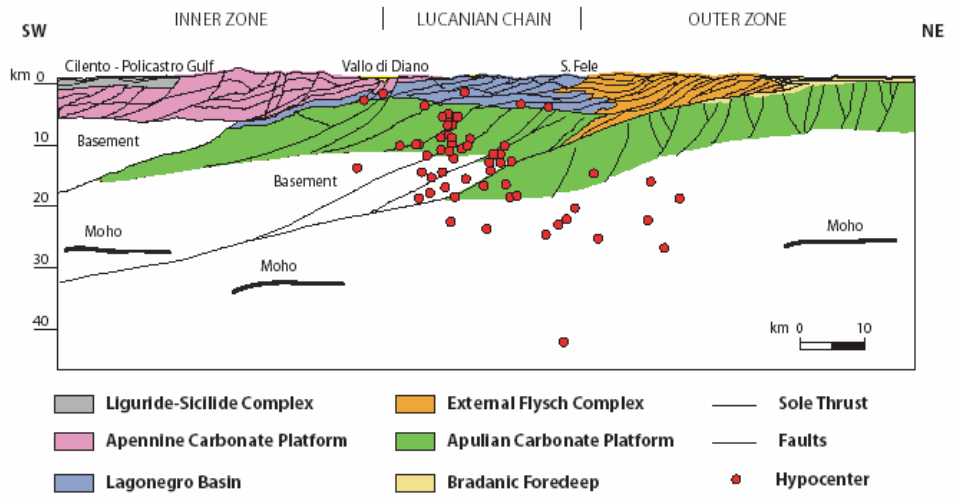
SW
INNER ZONE
LUCANIAN CHAIN
OUTER ZONE
NE
km 0
Cilento - Policastro Gulf
Vallo di Diano
S. Fele
10
Basement
Basement
20
Moho
Moho
Moho
30
40
km 0
10
Liguride-Sicilide Complex
Apennine Carbonate Platform
Lagonegro Basin
External Flysch Complex
Apulian Carbonate Platform
Bradanic Foredeep
Sole Thrust
Faults
Hypocenter

FIGURE 9